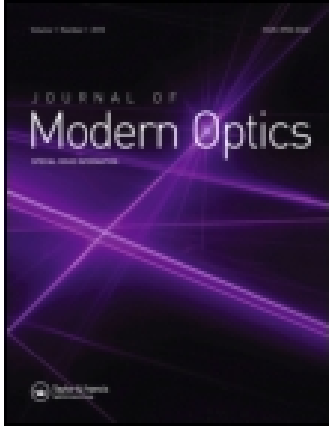


This article was downloaded by: [Shanghai Jiaotong University]

On: 13 July 2014, At: 19:55

Publisher: Taylor & Francis

Informa Ltd Registered in England and Wales Registered Number: 1072954 Registered office: Mortimer House, 37-41 Mortimer Street, London W1T 3JH, UK



## Journal of Modern Optics

Publication details, including instructions for authors and subscription information:

<http://www.tandfonline.com/loi/tmop20>

### Influence of slanted guiding layer on reflection curve and sensitivity for air-gap displacement sensor

Lin Chen<sup>a</sup>, Zhaoxiang Cheng<sup>a</sup> & Yiming Zhu<sup>a</sup>

<sup>a</sup> Shanghai Key Lab of Modern Optical System, Engineering Research Center of Optical Instrument and System, Ministry of Education, University of Shanghai for Science and Technology, Shanghai, China

Published online: 01 May 2014.



[Click for updates](#)

To cite this article: Lin Chen, Zhaoxiang Cheng & Yiming Zhu (2014) Influence of slanted guiding layer on reflection curve and sensitivity for air-gap displacement sensor, Journal of Modern Optics, 61:11, 938-942, DOI: [10.1080/09500340.2014.914594](https://doi.org/10.1080/09500340.2014.914594)

To link to this article: <http://dx.doi.org/10.1080/09500340.2014.914594>

PLEASE SCROLL DOWN FOR ARTICLE

Taylor & Francis makes every effort to ensure the accuracy of all the information (the "Content") contained in the publications on our platform. However, Taylor & Francis, our agents, and our licensors make no representations or warranties whatsoever as to the accuracy, completeness, or suitability for any purpose of the Content. Any opinions and views expressed in this publication are the opinions and views of the authors, and are not the views of or endorsed by Taylor & Francis. The accuracy of the Content should not be relied upon and should be independently verified with primary sources of information. Taylor and Francis shall not be liable for any losses, actions, claims, proceedings, demands, costs, expenses, damages, and other liabilities whatsoever or howsoever caused arising directly or indirectly in connection with, in relation to or arising out of the use of the Content.

This article may be used for research, teaching, and private study purposes. Any substantial or systematic reproduction, redistribution, reselling, loan, sub-licensing, systematic supply, or distribution in any form to anyone is expressly forbidden. Terms & Conditions of access and use can be found at <http://www.tandfonline.com/page/terms-and-conditions>

## Influence of slanted guiding layer on reflection curve and sensitivity for air-gap displacement sensor

Lin Chen, Zhaoxiang Cheng and Yiming Zhu\*

Shanghai Key Lab of Modern Optical System, Engineering Research Center of Optical Instrument and System, Ministry of Education, University of Shanghai for Science and Technology, Shanghai, China

(Received 19 February 2014; accepted 31 March 2014)

We investigate the influence of slanted guiding layer on reflection curves and sensitivity for air-gap optical waveguide structures. The theoretical analysis method is based on the interference between multiple light beams in the slanted guiding layer. The main relative characteristics of reflection curves and sensitivity as a function of inclination angle of slanted air-gap have been demonstrated in detail for symmetrical metal-cladding waveguide (SMCW) and Fabry–Pérot (FP) system. Results show that the sensitivity of SMCW with millimeter air-gap is more influenced by inclination angle than that of FP system. When inclination angle is larger than 10  $\mu$ rad, the reflection curve shows serious distortion for all waveguide configurations.

**Keywords:** air-gap displacement sensor; slanted guiding layer; Fabry–Pérot system

### 1. Introduction

Attenuated total reflectance (ATR) is a well-established technique for the excitation of optical surface modes, which was based on the method of frustrated total reflection presented by Otto for the first time [1]. The simplicity and the high sensitivity of ATR have allowed researchers to develop a variety of sensors for diverse applications [2]. Recently, researchers have found that using the ATR method the ultrahigh order-guided modes can be excited in symmetrical metal-cladding waveguides (SMCWs) which have much higher sensitivity than ordinary Fabry–Pérot (FP) system [3–6]. For optical intensity measurement based on the ATR technique, some important additional factors such as optical beam's diameter and surface roughness which may result in ATR profile distortion have been fully discussed [7–9]. Moreover, for sensors based on SMCW structure in the real situation, the sample cell or air-gap which serves as the guiding layer of the waveguide sensor is sealed by a spacer sandwiched between two gold films that are deposited on glass substrates/prism. The thickness of the guiding layer is governed by the thickness of the spacer [3,6]. So the top and bottom interfaces of the guiding layer cannot be treated as ideally parallel to each other due to the difference of stress on spacers. Thus the influence of slanted guiding layer should be taken into consideration for quantitative results. However, for slanted guiding layer, the phase velocity of the in-plane incident wave cannot match the velocity of an optical-guided

mode. As a consequence, the reflected power as a function of the angle of incidence does not follow the Fresnel reflection coefficient exactly. In this paper, we analyze the reflection curve distortion on optical waveguide with the slanted guiding layer. To calculate the reflectivity by considering the slanted guiding layer, we use the recently established theory [10,11] which shows that the physical mechanism of ATR is optical tunnel effect resulting from the interference between multiple reflections inside the slanted guiding layer. Then the influence of the slanted guiding layer on reflection curves and sensitivity is evaluated for different air-gap waveguide configurations: SMCW with different air-gap thicknesses (1000 and 108  $\mu$ m) and traditional FP system. Our results can also be expanded to analyze the Goos–Hänchen effect in slanted waveguide systems both in optical [12–15] and terahertz [16–18] range.

### 2. Theoretical model

We consider the case of the typical four-layer system. The guiding layer is sandwiched by the thin coupling layer and the substrate which acts as the reflecting panel. By employing the Fresnel formulas, one can write the reflectivity  $R$  as [5]

$$R(\theta_i) = \left| \frac{r_{12} + r_{234} \exp(2ik_2s)}{1 + r_{12}r_{234} \exp(2ik_2s)} \right|^2 \quad (1)$$

with

\*Corresponding author. Email: [ymzhu@usst.edu.cn](mailto:ymzhu@usst.edu.cn)

$$r_{234} = \frac{r_{23} + r_{34} \exp(2i\kappa_3 d)}{1 + r_{23}r_{34} \exp(2i\kappa_3 d)}, \quad (2)$$

where

$$\kappa_i = \left( (k_0 n_i)^2 - \beta^2 \right)^{1/2} \quad (3)$$

here,  $s$  and  $d$  are the thicknesses of the coupling layer and guiding layer, and  $r_{ij}$  is the complex Fresnel reflection coefficient for the boundary between media  $i$  and  $j$ .  $n_i$  and  $\kappa_i$  are the dielectric permittivity and the normal component of the wave vector at media  $i$ , respectively. Subscripts 1, 2, 3, and 4 refer to the dielectric layer, the coupling layer, the guiding layer, and the substrate, respectively.  $k_0 = 2\pi/\lambda$  is the wavenumber in vacuum and  $\beta$  is the propagation constant of the guided modes.

Now we consider the case of the slanted guiding layer with plane surface inclined at a small angle  $\phi$ , as schematically drawn in Figure 1. Suppose the wave is incident at the angle  $\theta_0$ . At the first surface, this wave is divided into two parts, one reflected with amplitude  $A_1$  and the other transmitted into the guiding layer with the angle of refraction  $\theta_1$  and propagation constant  $\beta_1$ . The latter wave is incident on the second surface at angle  $\varphi_1$ , and is thereby reflected back into the guiding layer. The process of division of the wave remaining inside the guiding layer continues as indicated in the Figure 1. The parameter  $\theta_n$  is the corresponding angle of the  $n$ th reflected light at the top surface;  $\varphi_n$  is the incident angle of the  $n$ th incident light at the bottom surface;  $d_n$  is the thickness of the guiding layer at the bottom position of the  $n$ th incident point;  $l_{nf}$  is the length from the  $n$ th reflected point at the top surface to the  $n$ th reflected point at the bottom surface in the  $z$  direction, and  $l_{nb}$  is the length from the  $n$ th reflected point at the bottom

surface to the  $(n+1)$ th reflected point at the top surface in the  $z$  direction. According to the geometrical optics rules, the  $\theta_n$ ,  $\varphi_n$ ,  $l_{nf}$ , and  $d_n$  can be expressed as:

$$\theta_n = \theta_1 - 2(n-1)\phi \quad (4)$$

$$\varphi_n = \theta_n - \phi \quad (5)$$

$$l_{nf} = d_n \tan \theta_n \quad (6)$$

$$l_{nb} = d_{n-1} \tan \theta_n \quad (7)$$

$$d_n = \frac{\cos \theta_1 \cos \phi}{\cos \varphi_n} d \quad (8)$$

where  $d$  is the thickness of the guiding layer at point O.

The vertical and horizontal wave vectors of the  $n$ th reflected light are defined as

$$\beta_n = k_0 n_3 \sin \theta_n \quad (9)$$

$$(\kappa_3)_n = k_0 n_3 \cos \theta_n \quad (10)$$

Let  $A$  be the complex amplitude of the electric vector of the incident wave and the complex amplitude of the reflected light in 1st-, 2nd-, and 3rd-order numbers  $A_1$ ,  $A_2$ , and  $A_3$  can be expressed as:

$$A_1 = Ar_{123}(\theta_0) \quad (11)$$

$$A_2 = At_{123}(\theta_0) \cdot \exp[i((\kappa_3)_1 + (\kappa_3)_2)d_1] \cdot r_{34}(\varphi_1) \cdot t_{321}(\theta_2) \cdot \frac{\exp[i(\beta_1 l_{1f} + \beta_2 l_{2b})]}{\exp[i\beta_2(l_{1f} + l_{2b})]} \quad (12)$$

$$A_3 = At_{123}(\theta_0) \cdot \exp[i((\kappa_3)_1 + (\kappa_3)_2)d_1] \cdot r_{34}(\varphi_1) \cdot r_{321}(\theta_2) \cdot \exp[i((\kappa_3)_2 + (\kappa_3)_3)d_2] \cdot r_{34}(\varphi_2) \cdot t_{321}(\theta_3) \cdot \frac{\exp[i(\beta_1 l_{1f} + \beta_2 l_{2b})]}{\exp[i\beta_2(l_{1f} + l_{2b})]} \cdot \frac{\exp[i(\beta_2 l_{2f} + \beta_3 l_{3b})]}{\exp[i\beta_3(l_{2f} + l_{3b})]} \quad (13)$$

where the reflection and transmission coefficients  $r_{321}$ ,  $r_{123}$ ,  $r_{34}$ ,  $t_{123}$ , and  $t_{321}$  are obtained as [10].

$$r_{321} = \frac{r_{32} + r_{21} \exp(2i\kappa_2 s)}{1 + r_{32}r_{21} \exp(2i\kappa_2 s)} \quad (14)$$

$$t_{321} = \frac{(1 - r_{12})(1 - r_{23}) \exp(i\kappa_2 s)}{1 + r_{12}r_{23} \exp(2i\kappa_2 s)} \quad (15)$$

$$r_{123} = \frac{r_{12} + r_{23} \exp(2i\kappa_2 s)}{1 + r_{12}r_{23} \exp(2i\kappa_2 s)} \quad (16)$$

$$t_{123} = \frac{(1 + r_{12})(1 + r_{23}) \exp(i\kappa_2 s)}{1 + r_{12}r_{23} \exp(2i\kappa_2 s)} \quad (17)$$

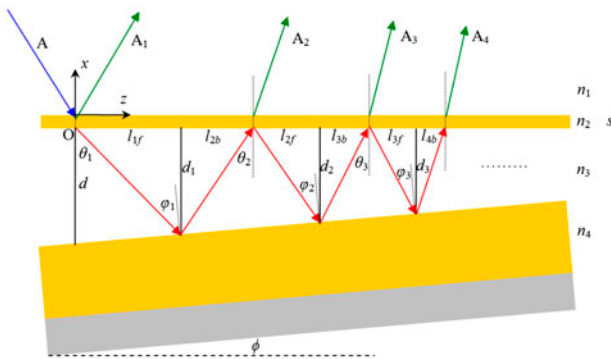


Figure 1. Interference model of laser beams in four-layer system with slanted guiding layer. (The colour version of this figure is included in the online version of the journal.)

If we define  $r_{321}(\theta_1) = 1$ , for  $n > 2$ ,  $A_n$  can be obtained from the following recurrence formula:

$$A_n = At_{123}(\theta_0) \cdot \left[ \prod_{j=1}^{n-1} B_j \right] \cdot t_{321}(\theta_n) \quad (18)$$

where

$$\begin{aligned} B_j &= r_{321}(\theta_j) \cdot \exp \left[ i \left( (\kappa_3)_j + (\kappa_3)_{j+1} \right) d_j \right] \cdot r_{34}(\varphi_j) \\ &\quad \cdot \frac{\exp [i(\beta_j l_{jf} + \beta_{j+1} l_{(j+1)b})]}{\exp [i\beta_{j+1} (l_{jf} + l_{(j+1)b})]} \\ &= r_{321}(\theta_j) \cdot r_{34}(\varphi_j) \\ &\quad \cdot \exp \left[ i \left( (\kappa_3)_j + (\kappa_3)_{j+1} \right) d_j + i(\beta_j - \beta_{j+1}) l_{jf} \right] \end{aligned} \quad (19)$$

Instituting Equations (4)–(10) into Equation (19), we can obtain

$$B_j = r_{321}(\theta_j) \cdot r_{34}(\varphi_j) \cdot \exp [ik_3 d \cdot (\cos 2\phi + \sin 2\phi \tan \theta_j + 1)] \quad (20)$$

In searching for an illustrative interpretation of the dip in the reflectivity, one thus naturally arrives at the concept of destructive interference of light beams reflected from the various interfaces of the film system of interest. The  $n$ th electric field of the  $n$ th reflected light can be found as

$$E_n = A_n \exp(i\beta_n z) \quad (21)$$

The overall reflected field is the sum of all superposed field:

$$E = \sum_n E_n = \sum_n A_n \exp(i\beta_n z) \quad (22)$$

Then reflectivity can be obtained

$$\begin{aligned} R &= \frac{1}{L} \frac{1}{|A|^2} \int_0^L \sum_n E_n \sum_m E_m^* dz \\ &= \frac{1}{L} \frac{1}{|A|^2} \int_0^L \sum_n \sum_m A_n A_m^* \exp(i(\beta_n - \beta_m)z) dz \end{aligned} \quad (23)$$

After integration, we can get:

$$R = \frac{1}{|A|^2} \left( \sum_n A_n A_n^* + \sum_n \sum_{m \neq n} A_n A_m^* \frac{\exp(i(\beta_n - \beta_m)L) - 1}{i(\beta_n - \beta_m)L} \right) \quad (24)$$

where  $L$  is the length of the multiple reflected regions in the  $z$  direction.

To illustrate the reliability of our result, we consider the example for incident light with a parallel guiding layer, i.e.  $\phi = 0$ . The amplitude of every sub-reflected light is obtained as:

$$A_1 = Ar_{123} \quad (25)$$

$$A_2 = At_{123} \cdot t_{321} \cdot r_{34} \cdot \exp(i2\kappa_3 d) \quad (26)$$

$$\begin{aligned} A_n &= At_{123} \cdot t_{321} \cdot r_{34} \cdot \exp(i2\kappa_3 d) \\ &\quad \cdot \{r_{321} \cdot r_{34} \cdot \exp(i2\kappa_3 d)\}^{n-2} \quad n > 2 \end{aligned} \quad (27)$$

The reflectivity Equation (20) can be simplified as

$$R = \frac{1}{|A|^2} \sum_n A_n \sum_n A_n^* \quad (28)$$

Through simple algebraic manipulations, we can get the conventional reflectivity as described in Equation (1). Note that the new form of the amplitude reflectivity, by one introducing a slanted guiding layer, applies not only to four-layer system but also to multi-layer waveguide with the slanted guiding layer.

### 3. Results and discussion

In this section, we give some quantitative results for reflection curves and their first differentials (sensitivity) for different values of the inclination angle. For the calculations, we considered two typical air-gap waveguide configurations: SMCW with different air-gap thicknesses ( $d = 1000$  and  $108 \mu\text{m}$ ) [3] and ordinary FP system ( $d = 1000 \mu\text{m}$ ). For SMCW, the thickness of the bottom gold film (substrate) is thick enough ( $400 \text{ nm}$ ) to serve as the reflected panel. However, we choose for this thickness also a  $40 \text{ nm}$  layer which is the same as the upper gold film ( $s = 40 \text{ nm}$ ) in principle a FP system is obtained. The other parameters are as follows:  $\lambda = 650 \text{ nm}$ ,  $n_1 = 1.73$

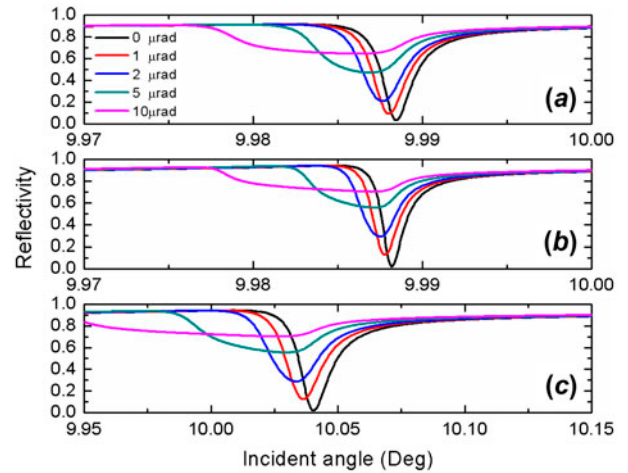


Figure 2. Plot of reflectivity as a function of incident angle for inclination angle  $\phi = 0, 1, 2, 5, 10 \mu\text{rad}$  with different waveguide structures: (a) FP system; (b) SMCW with  $d = 1000 \mu\text{m}$ ; (c) SMCW with  $d = 108 \mu\text{m}$ . The waveguide parameters are as follows:  $\lambda = 650 \text{ nm}$ ,  $n_1 = 1.73$  (glass prism),  $\epsilon_2 = n_2^2 = -11 + 1.0i$  (gold film),  $n_3 = 1$  (air gap),  $n_4 = n_2$ ,  $s = 40 \text{ nm}$  (by use of Equation (24)). (The colour version of this figure is included in the online version of the journal.)

(glass prism),  $\varepsilon_2 = n_2^2 = -11 + 1.0 i$  (gold film),  $n_3 = 1$  (air gap),  $n_4 = n_2$ ,  $s = 40$  nm, and  $L = 10$  mm.

Figure 2 shows the reflectivity  $R$  as a function of the incident angle  $\theta_i$  for inclination angle  $\phi = 0, 1, 2, 5,$  and  $10 \mu\text{rad}$  for FP system and SMCW configuration with  $d = 108$  and  $1000 \mu\text{m}$ . Taking SMCW with  $d = 108 \mu\text{m}$  as an example (Figure 2(c)), we focus on the dependence of three main parameters of the curves (the synchronism angle position  $\theta_{\text{syn}}$ , the value of minimum  $R_{\text{min}}$ , the full width half maximum of the resonance dip FWHM) on the inclination angle  $\phi$ . First, with increase of  $\phi$ , the synchronous angle begins to shift towards the smaller incident angle side. The position of the minimum is shifted by 4, 7, 11, and 13 mrad for  $\phi$  is 1, 2, 5, and  $10 \mu\text{rad}$ , respectively, from the position of an ideal non-parallel waveguide ( $\phi = 0$ ). Moreover, by increasing  $\phi$ , the reflectivity at resonance dip rises. The reflectivity minimum is approximately 6, 15, 28, and 35 times larger than that for an ideal plane wave for the respective value of  $\phi$ . Finally, the FWHM of the resonance curve is  $0.0156^\circ$ ,  $0.0182^\circ$ ,  $0.0246^\circ$ ,  $0.0516^\circ$ , and  $0.092^\circ$  for the respective values of  $\phi$  is 0, 1, 2, 5, and  $10 \mu\text{rad}$ . It is clear from Figure 2 that when  $\phi$  is larger than  $10 \mu\text{rad}$ , the reflection curve would dramatically disappear and lose its characteristics.

For the purpose of comparison, we also calculate the  $\Delta\theta_{\text{syn}}$  curves, the  $\Delta R_{\text{min}}$  curves, and the  $\Delta\text{FWHM}$  curves for FP system and different air-gap SMCW configurations with the variation of the inclination angle  $\phi$  from 0 to  $10 \mu\text{rad}$ , as shown in Figure 3(a)–(c). Here, the symbol  $\Delta$  represents the offset from the respective parameter at  $\phi = 0$  in order to remove the differences of initial values. First, in Figure 3(a), we can see that the thinner air-gap gives the larger  $\Delta\theta_{\text{syn}}$  value at all values of  $\phi$ . The reason is that the synchronism angle  $\theta_{\text{syn}}$  is determined from the propagation constant of guided mode, which is strongly dependent on the air-gap thickness  $d$  according to the phase-matching condition for the coupling of radiative modes to the guided mode near a resonance. For the variation of  $d$  induced by  $\phi$ , the larger  $\Delta\theta_{\text{syn}}$  can be obtained using a thinner guiding layer. In addition, for a fixed  $d$  value ( $1000 \mu\text{m}$ ),  $\Delta\theta_{\text{syn}}$  of SMCW is slightly smaller than that of FP system, which is due to the energy coupling at both sides of thin metal films in FP system. Second, Figure 3(b) shows that the curve for  $\Delta R_{\text{min}}$  vs.  $\phi$  of SMCW with  $d = 108 \mu\text{m}$  (blue line) coincides with that of SMCW with  $d = 1000 \mu\text{m}$  (red line), owing to the fact that  $R_{\text{min}}$  can be expressed as  $[(1 - \eta)/(1 + \eta)]^2$  and is independent with  $d$  (here  $\eta = \text{Im}(\beta^0)/\text{Im}(\Delta\beta^d)$ , where  $\text{Im}(\beta^0)$  and  $\text{Im}(\Delta\beta^d)$  represent intrinsic

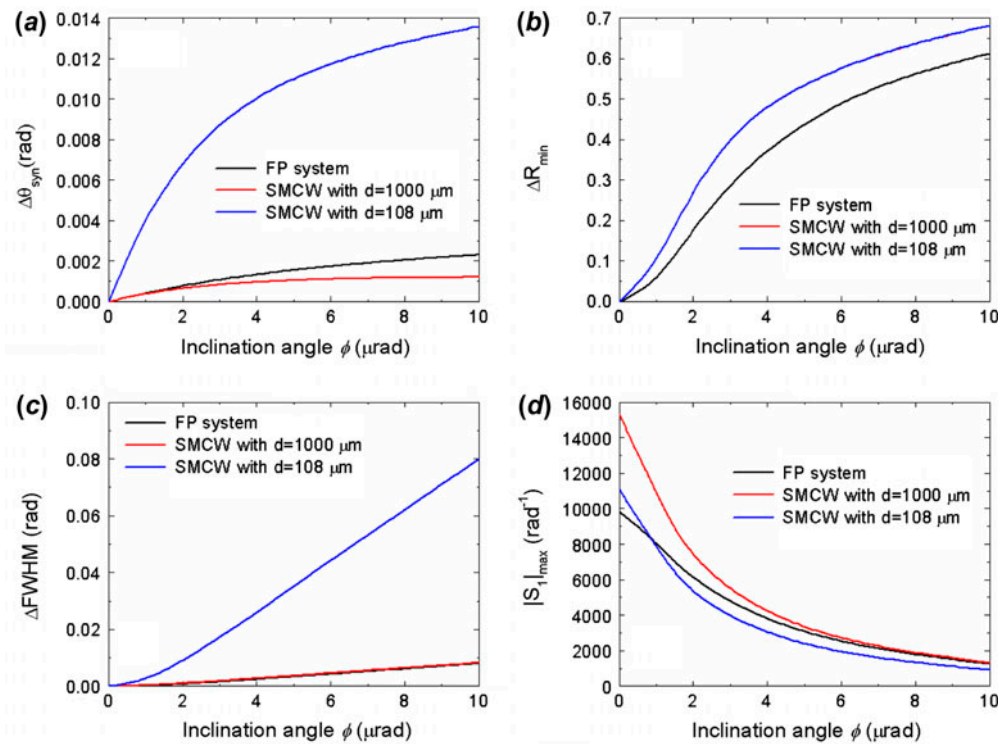


Figure 3. Main characteristics of reflection curves as a function of inclination angle  $\phi$  for different waveguide configurations: (a) the relative position of the minimum, (b) the relative value at the minimum, (c) the relative FWHM of curves, (d) the absolute maximum of the sensitivity  $S_1$ . (The colour version of this figure is included in the online version of the journal.)

damping and radiation damping, respectively, and their expressions can be found in [19]). Moreover, the values  $R_{\min}$  of SMCW is larger than those of FP system (black line) at all values of  $\phi$  in Figure 3(b), because the energy of the incident light will leak from the bottom metal layer which causes the reflected light intensity to decrease in FP system. Third, from Figure 3(c) we can see that the larger  $\Delta\text{FWHM}$  for SMCW can be obtained using a thinner guiding layer (108  $\mu\text{m}$ ) with the variation of  $\phi$ . This is because FWHM is determined by waveguide loss. The smaller the air-gap thickness, the larger the loss, and the broader the FWHM.

The sensitivity  $S_1$ , which is defined as the first differential  $dR/d\theta$  (as expressed in Equation (1) of [3]), is a key parameter to evaluate the performance of the sensor. As a final numerical result, we compare the dependence of absolute maximum sensitivity  $|S_1|_{\max}$  on  $\phi$  with different waveguide configurations, as shown in Figure 3(d). Several remarks can be made about the evolution of  $|S_1|_{\max}$  relative to  $\phi$ . First,  $|S_1|_{\max}$  clearly decreases as an increasing  $\phi$ .  $|S_1|_{\max}$  for SMCW with  $d=108\ \mu\text{m}$  (blue line) decreases 27, 55, and 82% when compared with that of a non-parallel waveguide for  $\phi$  of 1, 2, and 5  $\mu\text{rad}$ , respectively. These decrements of the  $|S_1|_{\max}$  will affect, in the same proportion, the maximum sensitivity of air-gap displacement sensor because it is proportional to  $|S_1|_{\max}$ . It is worth noting that the largest value of  $|S_1|_{\max}$  for SMCW with  $d=1000\ \mu\text{m}$  (red line) can be obtained. According to the dispersion equation of ultra-high-order modes in an SMCW [19], the mode number is proportional to the air-gap thickness  $d$ . Since the FWHM of the reflection dips decreases as the mode number increases (see Figure 3(c)) and a small FWHM value is expected for achieving higher sensitivity, the sensitivity for SMCW with  $d=1000\ \mu\text{m}$  is larger than that with  $d=108\ \mu\text{m}$ . Additionally, the sensitivity of SMCW with  $d=1000\ \mu\text{m}$  decreases faster than that of FP system. When  $\phi > 4\ \mu\text{rad}$  and  $d$  is fixed, the sensitivity curves of FP system (black line) and SMCW (red line) almost overlap, indicating that SMCW has no advantage in sensitivity. As a result, the inclination angle represents a significant influence when high-resolution air-gap displacement measurements are desirable or when one aims to achieve the designed sensitivity of the displacement sensor [3].

#### 4. Conclusion

In conclusion, we focus on the effects of the slanted guiding layer on the resonance curve and the sensitivity of air-gap displacement sensors that are based on the SMCW with different air-gap thicknesses and FP system. A theoretical model based on the interference between

multiple reflections inside the slanted guiding layer is built. We calculate the reflection curves and their first differentials of the air-gap displacement sensor considering the slanted guiding layer. Results show that the inclination angle of the guiding layer is a crucial parameter in the reflection curve and sensitivity should be taken into account in order to evaluate the sensitivity of high-resolution displacement sensor.

#### Funding

This work was partly supported by the National Program on Key Basic Research Project of China [973 Program, 2014CB339806]; Basic Research Key Project [12JC1407100]; Major National Development Project of Scientific Instrument and Equipment [2011YQ150021], [2012YQ14000504], the Key Scientific and Technological Project of Shanghai Municipality [12142200100]; Shanghai Rising-Star Program [14QA1403100]; Program of Shanghai Subject Chief Scientist [14XD1403000]; National Natural Science Foundation of China [11174207], [61138001], [61007059], [61205094], [61307126], and the Leading Academic Discipline Project of Shanghai Municipal Government [S30502].

#### References

- [1] Otto, A. *Z. Phys.* **1968**, *216*, 398–410.
- [2] Li, C.T.; Yen, T.J.; Chen, H.F. *Opt. Express* **2009**, *17*, 20771–20776.
- [3] Chen, F.; Cao, Z.Q.; Shen, Q.S.; Deng, X.X.; Duan, B.M.; Yuan, W.; Sang, M.H.; Wang, S.Q. *Appl. Phys. Lett.* **2006**, *88*, 161111–2.
- [4] Zhou, J.H.; Deng, X.X.; Cao, Z.Q.; Shen, Q.S.; Wei, W.; Zhang, Z.J.; Xie, S.X. *Appl. Phys. Lett.* **2006**, *88*, 021106–3.
- [5] Chen, L.; Cao, Z.Q.; Shen, Q.S.; Deng, X.X.; Ou, F.; Feng, Y.J. *J. Lightwave Technol.* **2007**, *25*, 539–543.
- [6] Wu, P.T.; Wu, M.C.; Wu, C.M. *J. Appl. Phys.* **2010**, *107*, 083111–8.
- [7] Villatoro, J.; García-Valenzuela, A. *Appl. Opt.* **1999**, *38*, 4837–4844.
- [8] Lee, C.-C.; Jen, Y.-J. *Appl. Opt.* **1999**, *38*, 6029–6033.
- [9] Kanso, M.; Cuenot, S.; Louarn, G. *J. Opt. A: Pure Appl. Opt.* **2007**, *9*, 586–592.
- [10] Liu, X.M.; Zhu, P.F.; Cao, Z.Q.; Shen, Q.S. *J. Opt. Soc. Am. B* **2006**, *23*, 353–357.
- [11] Liu, X.M.; Yang, Q.F.; Qiao, Z.; Li, T.K.; Zhu, P.F.; Cao, Z.Q. *Opt. Commun.* **2010**, *283*, 2681–2685.
- [12] Chen, L.; Cao, Z.Q.; Ou, F.; Li, H.G.; Shen, Q.S.; Qiao, H.C. *Opt. Lett.* **2007**, *32*, 1432–1434.
- [13] Salasnich, L. *Phys. Rev. A* **2012**, *86*, 055801–4.
- [14] Chen, L.; Zhu, Y.M.; Peng, Y.; Zhuang, S.L. *J. Opt.* **2010**, *12*, 075002–6.
- [15] Chen, L.; Liu, X.B.; Cao, Z.Q.; Zhuang, S.L. *J. Opt.* **2011**, *13*, 035002–8.
- [16] Chen, L.; Xu, J.M.; Gao, C.M.; Zang, X.F.; Cai, B.; Zhu, Y.M. *Appl. Phys. Lett.* **2013**, *103*, 251105–4.
- [17] Chen, L.; Zhu, Y.M.; Zang, X.F.; Cai, B.; Li, Z.; Xie, L.; Zhuang, S.L. *Light Sci. Appl.* **2013**, *2*, e60.
- [18] Chen, L.; Gao, C.M.; Xu, J.M.; Zang, X.F.; Cai, B.; Zhu, Y.M. *Opt. Lett.* **2013**, *38*, 1379–1381.
- [19] Chen, L.; Zhu, Y.M.; Zhang, D.W.; Cao, Z.Q.; Zhuang, S.L. *Chin. Phys. B* **2009**, *18*, 4875–4880.